 

https://doi.org/10.1070/QEL17550

# Deposition of silver on the surface of microparticles of zirconium and molybdenum oxides during their synthesis by laser ablation in liquid

M.M. Malikov, G.E. Val'yano, T.I. Borodina

*Abstract.* **The deposition of silver on the surfaces of micro- and nanoparticles of zirconium, molybdenum, and their oxides, obtained by laser ablation of pure metals in aqueous solutions of silver nitrate, is investigated experimentally. Different irradiation regimes and reagent concentrations are approved. The experimental results indicate a possibility of continuous or partial coating (decorating) with silver the surfaces of nanostructures of oxides of the aforementioned metals; using such systems as substrates, one can increase the Raman scattering amplitude. Silver-coated zirconium and molybdenum oxides can be applied in the diagnostic techniques based on the phenomenon of surface-enhanced Raman scattering.**

***Keywords:*** *laser ablation in liquid, nanostructures, oxides, zirconium, molybdenum, silver deposition.*

## 1. Introduction

To implement the highly sensitive method for determining the composition of various materials (analytes), based on the phenomenon of surface-enhanced Raman scattering (SERS), one must find materials (the so-called substrates) with a well-developed nano- or microstructured surface contacting with analyte molecules [1, 2]. Examples of such substrates are nanostructures of transition metal oxides, which have high chemical durability, thermal stability, and relatively low cost [3–5] in comparison with substrates involving nanoparticles of gold, silver, etc. Metal substrates with a high electrical conductivity are known to be characterised by plasmonic SERS mechanism [3, 6], which increases the scattered signal amplitude by a factor of $10^{12}-10^{14}$. Substrates based on transition metal oxides exhibit a much lower SERS enhancement factor (on the order of $10^4-10^8$). The enhancement factor can be increased significantly by depositing metals with a high electrical conductivity (silver, gold, etc.) on the surface of oxide substrates of [7, 8]. These substrates can be widely used in practice, in particular, in diagnostics of two-phase high-speed gas-dynamic flows [9, 10].

**M.M. Malikov, G.E. Val'yano, T.I. Borodina** Joint Institute for High Temperatures, Russian Academy of Sciences, Izhorskaya ul. 13, stroenie 2, 125412 Moscow, Russia;
e-mail: mmalikov@oivtran.ru

Received 4 March 2021
*Kvantovaya Elektronika* **51** (6) 544–548 (2021)
Translated by Yu.P. Sin'kov

It is known [11, 12] that core–shell nanoparticles can be obtained by irradiating a colloid containing a mixture of prepared nanoparticles of two different metals with significantly different melting temperatures with high-power laser pulses. After laser-beam-induced melting of particles, a particle with a lower melting temperature can envelop a particle with a higher melting temperature when the latter hardens upon cooling. When the surface of semiconductor nanoparticles must be coated with high-conductivity metals, commercial nanopowders of oxides and aqueous salt solutions (reagents) – metal dopant suppliers – are often used to this end (see, e.g., [8]). Such mixtures are irradiated by short laser pulses.

In experiments we actually combine the formation of submicron particles of metal oxides with the coating of their surface by silver, performing laser ablation of metal targets in an aqueous solution of reagent. This approach, implying one-stage synthesis of metal and oxide particles with their coating by noble metals or other elements that are present in liquid, has been applied for a long time; it was discussed in detail in a number of reviews (see, e.g., [13–15]). The irradiation of a target in liquid by a laser pulse leads to the formation of plasma–vapor microbubbles, in which high temperature and pressure are obtained for a short time, and complex physicochemical processes with participation of reagents occur. As a result, a colloidal solution is formed, which consists of individual micro- and nanoparticles and their conglomerates [14–16]. Previously [17–19], we implemented ablation of transition metals Cu, Zn, Zr, Mo, W, and V in pure water and investigated the compositions and morphology of the particles formed. In this study, we chose Zr and Mo from this series to perform the first experiments on 'doping' oxide microparticles and compare the results of their ablation in pure water and in an aqueous solution of silver nitrate.

## 2. Experimental setup and diagnostics of nanoparticle properties

The synthesis of nanostructures of zirconium and molybdenum oxides and their doping were performed by laser ablation of pure metals in water with silver nitrate solution added. The experimental bench was described in [17]. It includes a repetitively pulsed copper vapour laser with radiation wavelengths of 510 and 578 nm, pulse duration ~20 ns, pulse repetition rate of 10 kHz, and average output power of 13–15 W. The radiation peak power and pulse energy were,

respectively, ~100 kW and 1 mJ. The laser beam was focused on the metal target surface by an achromatic objective with a focal length $f = 190$ mm, which provided an irradiation spot ~40 μm in size. A target ~5 mm thick was placed on the bottom of a cell filled with distilled water or an $AgNO_3$ aqueous solution (filling volume of 4 mL). The cell was rotated with a speed of ~2 rpm, so that the irradiation spot moved over the target surface. The nanomaterial samples designed for analysis were prepared from a colloid by the spin coating technique and subsequent precipitate drying on glass or copper substrates.

The microstructure and elemental composition of preparations were studied with a scanning electron microscope (SEM) Nova NanoSem 650, equipped with EDS-analysis system EDAX to record and process characteristic X-ray radiation (CXR) spectra. In addition, an annular backscatter electron detector was used, which provides contrast (in average atomic numbers) images of microstructure elements on relief surfaces. No conducting coating was deposited on preparations before the analysis. Note that the diameter of CXR generation region was ~1.5 μm in this case; therefore, the EDS data gave an estimate of elemental content averaged over the volume of CXR generation region in a preparation. The phase compositions of preparations were studied by X-ray diffraction (XRD) analysis on a SmartLab (Rigaku) system according to the standard technique.

## 3. Study of the Zr and Mo ablation and discussion of results

Ablation of zirconium and molybdenum was performed in $AgNO_3 + H_2O$ solutions with silver nitrate molar concentrations $C_m = 6 \times 10^{-3}$, $6 \times 10^{-4}$, and $6 \times 10^{-5}$ mol $L^{-1}$. Distilled water was used. The target irradiation time $\tau_{em}$ was varied from 20 min to 3 h. The solution with a concentration $C_m = 6 \times 10^{-5}$ turned out to be too weak, and silver was barely observed in ablation preparations. When using the solution with $C_m = 6 \times 10^{-3}$, the amount of released silver was too much, especially at large (2–3 h) $\tau_{em}$ values. We present below the results of the experiments performed under more optimal conditions: at a solution concentration $C_m = 6 \times 10^{-4}$ and irradiation time $\tau_{em} \approx 30-50$ min. Note that the metal targets were additionally weighed before and after ablation in some experiments. For example, at $\tau_{em} = 2$ h, the decrease in the masses of Zr and Mo targets was about 1 and 2 mg, respectively, while at $\tau_{em} \approx 30$ min the corresponding decrease in mass was approximately twice as low. Thus, the weight content of the ablation products entering the working volume of the cell filled with 4 mL initial solution was estimated.

SEM images (Fig. 1) exhibit the morphology of the structures of the colloid precipitate formed as a result of zirconium ablation. It can be seen that the main components of the preparation are as follows:

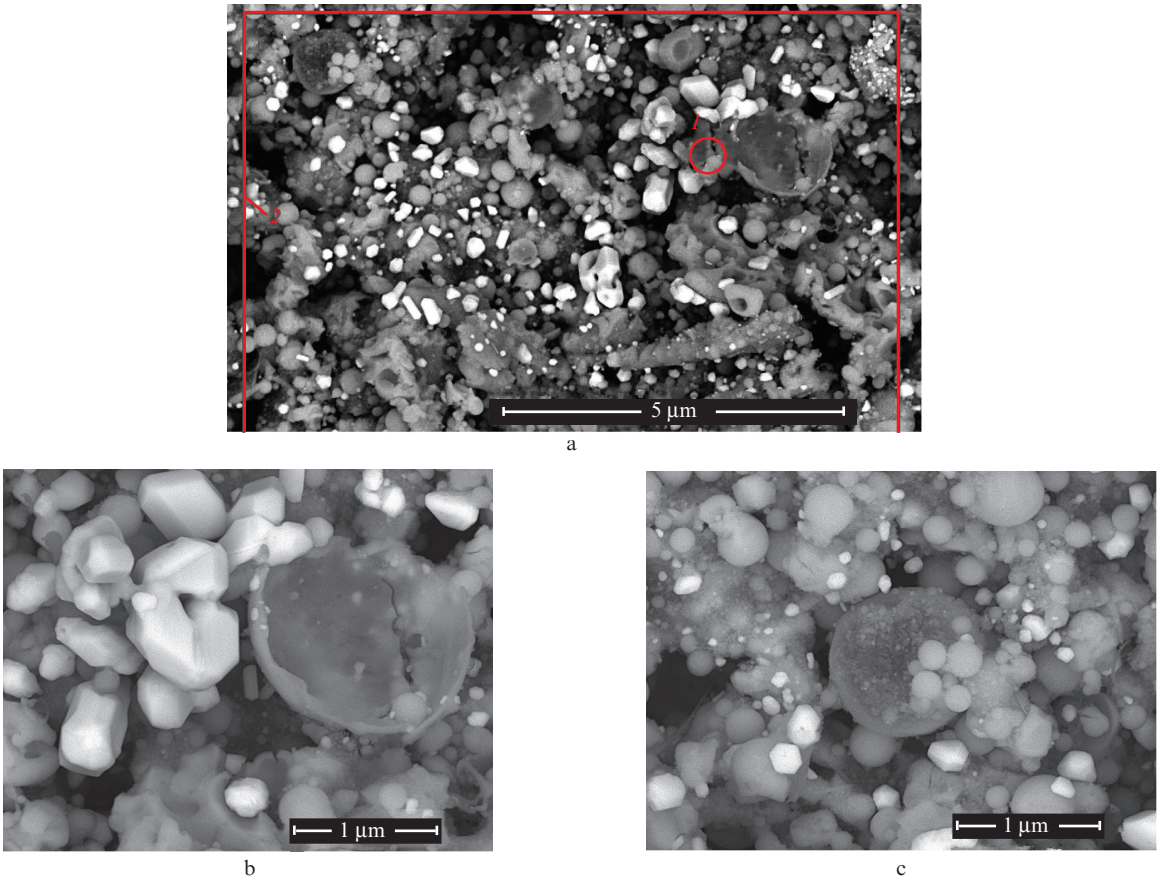


**Figure 1.** (a) Microstructures of characteristic portions of the ablation product for the Zr + $AgNO_3$ + $H_2O$ mixture (backscattered-electron image) and (b, c) fragments of this image at higher magnifications; $\tau_{em} \approx 30$ min. The red solid lines outline the first and second regions of EDS analysis.

(i) grey (basically hollow) microspheres with different surface defects (~100–1000 nm in diameter) and their fragments ('shells') (Fig. 1a);

(ii) bright and light-coloured polyhedral particles of submicron sizes, nonuniformly distributed in a preparation (Fig. 1b); and

(iii) nanoparticles with linear sizes of ~10–30 nm, covering separate microspheres with a thin layer (Fig. 1c).

An analysis of the EDS data on the elemental composition indicates that the main elements in 'bright and light-coloured' particles in some CXR generation regions (~1.5 μm in diameter) is Ag, whereas the main elements in 'grey' particles are Zr and O. For example, in bright region *1* with an area of ~1 $\mu m^2$, an estimation of averaged Ag weight content yields ~90% (Fig. 2a). Averaging over a larger area (~100 $\mu m^2$) in region *2* yields a much lower Ag content: ~17% (Fig. 2b).

With a further increase in averaging area (approximately to 600 $\mu m^2$), the Ag weight content decreases and ranges from 8% to 12%.

An XRD analysis of the preparation (Fig. 3a) showed the presence of crystalline zirconia $ZrO_2$, metallic silver Ag, and silver oxide $Ag_2O$. Zirconia is represented by two modifications: monoclinic and tetragonal. Tetragonal $ZrO_2$ has the following lattice parameters: $a = 0.5085 \pm 0.0001$ nm and $c = 0.5159 \pm 0.0001$ nm. The average size of coherent-scattering regions (CSRs) in all recorded phases is no less than 100 nm. The volume contents of monoclinic $ZrO_2$ and tetragonal $ZrO_2$ in the crystalline part of precipitate are 41% and 51%, respectively; the contents of metallic silver and oxide $Ag_2O$ are 5% and 3%, respectively.

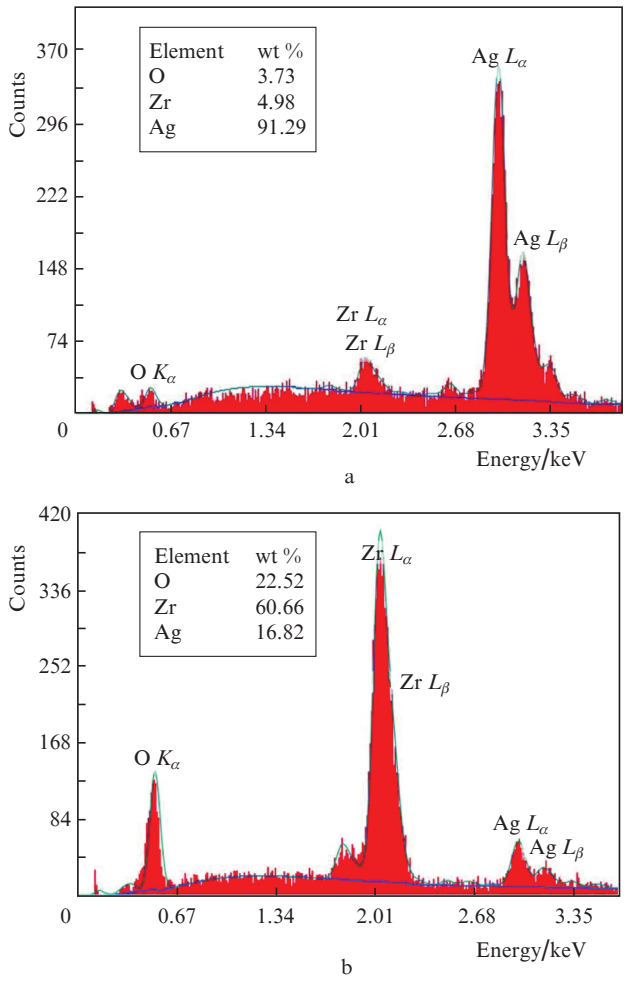


**Figure 2.** EDS spectra and elemental composition of the ablation products for the Zr + $AgNO_3$ + $H_2O$ mixture in regions (a) *1* and (b) *2*, shown in Fig. 1a. The weight contents of elements are indicated in the insets.

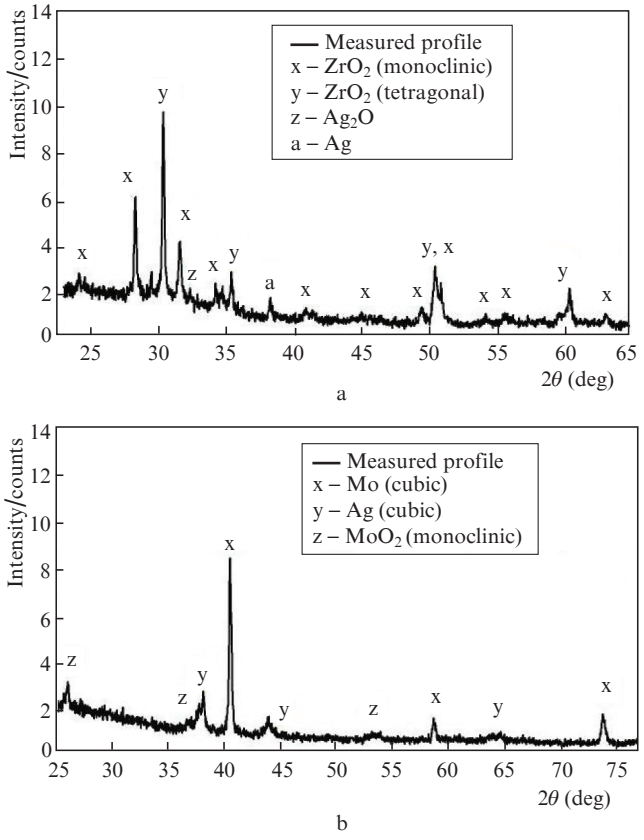


**Figure 3.** XRD patterns of ablation products: (a) zirconium and (b) molybdenum in an aqueous solution of silver nitrate.

Comparing the EDS and XRD data, we can conclude that the dominant (~90 vol %) compounds in this preparation are monoclinic and tetragonal $ZrO_2$, which are concentrated to a great extent in microspheres. The tetragonal structure of zirconia is likely stabilised by silver oxide $Ag_2O$. Since the electron-probe charging of microstructure elements was insignificant, one can suggest that microspheres, nanoparticles, and their conglomerates are coated by a thin layer of conducting material, presumably Ag.

The morphology of the microstructures of molybdenum ablation products in an aqueous solution of silver nitrate is presented in Fig. 4. A preparation was deposited on a copper substrate. SEM images were recorded in both secondary- and backscattered-electron regimes. The images show that the main components of the preparation are as follows:

(i) Microspheres, mainly 500–3000 nm in diameter, with pronounced segregations on their surfaces (Figs. 4a, 4c). These segregations are especially clear and pronounced in the

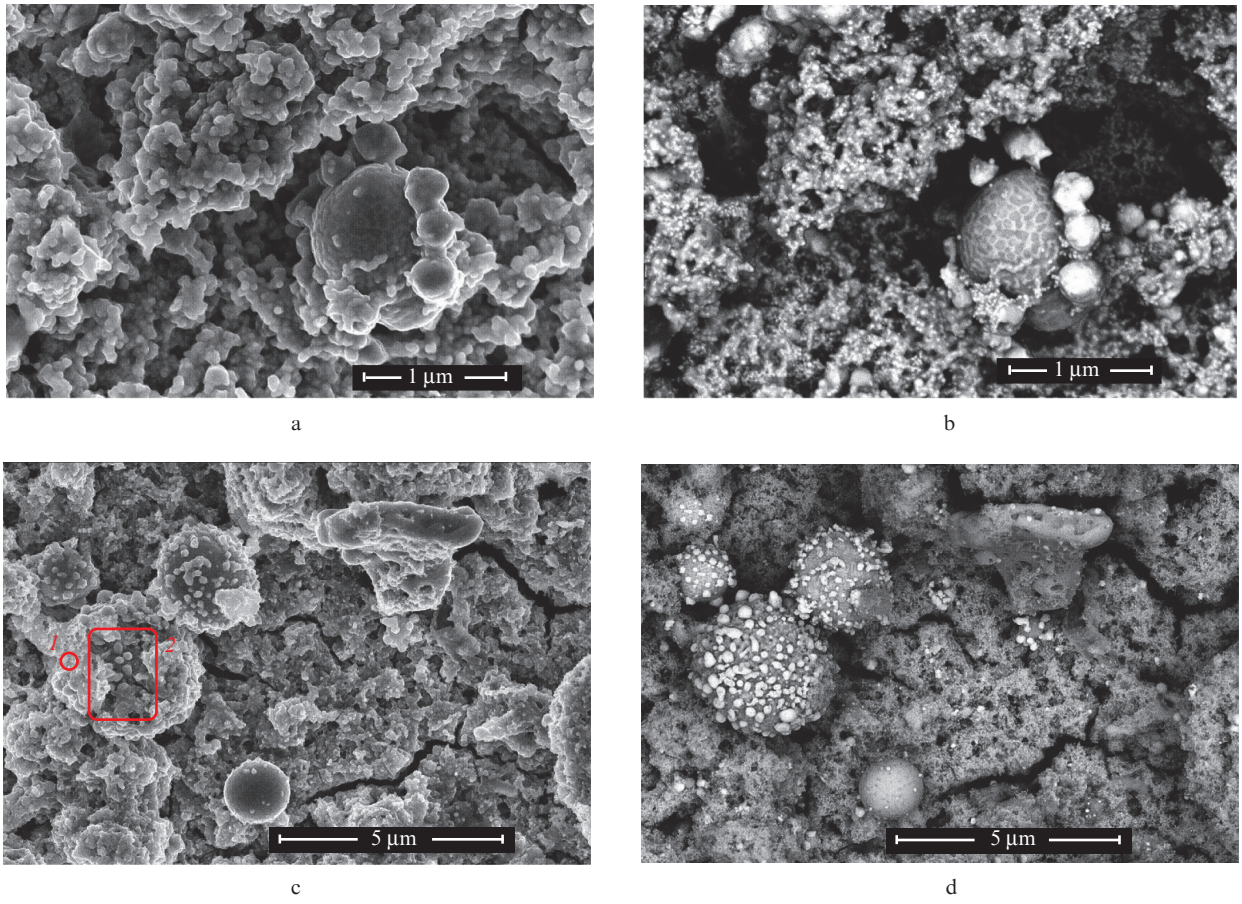


**Figure 4.** Images of the microstructure of characteristic regions of the laser ablation product for the Mo + $AgNO_3$ + $H_2O$ mixture, recorded in the (a, c) secondary-electron and (b, d) backscattered-electron regimes; $\tau_{em} \approx 50$ min. The red solid lines outline the EDS-analysis regions on the surface of a large microsphere.

SEM images recorded using an annular backscatter electron detector (Figs 4b, 4d).

(ii) Agglomerates of particles with a transverse size of ~30–50 nm, covering a copper substrate and saturated with discrete nanoscale bright segregations (Fig. 4b).

The results of the EDS analysis of the elemental composition of molybdenum ablation products are shown in Fig. 5. It can be seen that the regions on microsphere surfaces with bright segregations contain Ag- and Mo-based phases. In region *1* (Fig. 4c) an immobile electron beam was positioned on an individual bright selection located on a microsphere. In this case, the EDS analysis showed maximum values of Ag weight content, which reached ~66% at a Mo content of ~19% (Fig. 5a). In region *2* with a scan area of ~8 μm$^2$, the averaged values of Ag and Mo weight contents on the microsphere surface were, respectively, 26% and 62% (Fig. 5b). The Ag content, averaged over the large preparation area (~700 μm$^2$), was estimated to be ~24 wt %.

It follows from Figs 4b and 4d that the coating of microstructures with a silver-based material is mainly of island type. This partial coating is similar to the decoration of nanoparticles with gold [8]. Note that the obtained data on the ablation with molybdenum differ significantly from the corresponding data on zirconium: in the latter case, along with intermittent coating of surfaces of some zirconia microspheres with particles of Ag-based phases, there is apparently a continuous coating of microparticles with aggregates of silver nanolayers.

The conclusions based on the EDS analysis are confirmed by the XRD data (Fig. 3b), which demonstrated the presence of three crystalline phases: two metals (Mo and Ag) and molybdenum oxide $MoO_2$. The volume contents of molybdenum, silver, and $MoO_2$ in the crystallised part of precipitate are, respectively, 84%, 10%, and 6%. Thus, more than 90 vol % of the crystallised part of dried precipitate is a conducting material: metallic phases of molybdenum and silver. This ratio of the metal and oxide components differs from the corresponding ratio for zirconium ablation, which was given above. The average CSR size is no less than 100 nm for molybdenum and 40 ± 2 nm for other phases.

Note that the XRD analysis in the experiments performed with both molybdenum and zirconium did not reveal the presence of crystallised hydroxide phases of target materials. However, it is not excluded that samples contain a small amount of some hydroxides in the amorphous state, which cannot be detected by the XRD method.

The XRD data indicate a very high degree of crystallisation of materials throughout the entire area of preparation in comparison with that obtained previously for their ablation in pure water [18, 19]. However, the crystallised parts of precipitates, both Mo- and Zr-based, obtained both in pure water and in an aqueous solution of silver nitrate, turned out to have similar morphologies: they were conglomerates of nanoparticles with a highly developed surface.

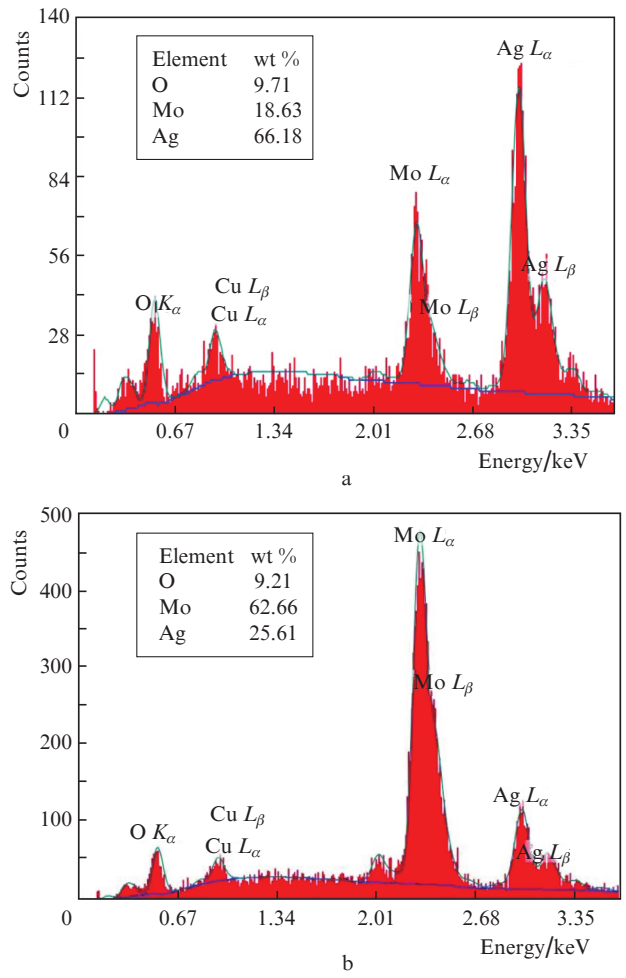


**Figure 5.** EDS spectra and elemental composition of the ablation products for the Mo + $AgNO_3$ + $H_2O$ mixture in regions (a) *1* and (b) *2*, presented in Fig. 4c.

## 4. Conclusions

The experimental results on laser ablation of Zr and Mo in an aqueous solution of silver nitrate showed a possibility of synthesising diverse conglomerates of nano- and microparticles, consisting of oxides of aforementioned metals, as well as pure metals. Under these conditions, the oxides can simultaneously be coated (decorated) with silver. These materials are of great practical interest, because the porous, highly developed surface of the nanostructures studied, coated by a conducting metal (Ag), indicates a possibility of achieving a high Raman enhancement coefficient with these materials used as substrates.

## References

1. Emel'yanov V.I., Koroteev N.I. *Usp. Fiz. Nauk*, **135**, 345 (1981) [*Sov. Phys. Usp*, **135**, 345 (1981)].
2. Zuev V.S. *Poverkhnostnye polyaritony i plazmony: spontannoe izluchenie atoma vblizi tela malogo razmera* (Surface Polaritons and Plasmons: Spontaneous Emission from an Atom near a Small Body) (Moscow: FIAN, 2006) p. 16.
3. Lombardi J.R., Birke R.L. *J. Phys. Chem.*, **118** (20), 11120 (2014).
4. Shan Cong, Yinyin Yuan, Zhigang Chen, Junyu Hou, Mei Yang, Yanli Su, Yongyi Zhang, Liang Li, Qingwen Li, Fengxia Geng, Zingang Zhao. *Nature Commun.*, **6**, 7800 (2015).
5. Wei Ji, Bing Zhao, Yukihiro Ozaki. *J. Raman Spectrosc.*, **47**, 51 (2016).
6. Yamamoto Yuko S., Tamitake Iton. *J. Raman Spectrosc.*, **47**, 78 (2016).
7. Pisarek M., Roguska A., Kudelski A., Holdinski M., Janik-Czachor M., Hnida K., Sulka G.D. *Vib. Spectrosc.*, **71**, 85 (2014).
8. Gurbatov S.O., Mincheva N., Ivamori S., Kulinich S.A., Kuchmizhak A.A. *Quantum Electron*, **50** (9), 855 (2020) [*Kvantovaya Elektron.*, **50** (9), 855 (2020)].
9. Varaksin A.Yu. *High Temperature*, **58** (5), 716 (2020).
10. Varaksin A.Yu. *High Temperature*, **57** (4), 555 (2019).
11. Barmina E.V., Shafeev G.A. *Quantum Electron*, **48** (7), 637 (2018) [*Kvantovaya Elektron.*, **48** (7), 637 (2018)].
12. Barmina E.V., Sukhov I.A., Viau G., Shafeev G.A. *ChemPhysChem.*, **18**, 1069 (2017).
13. Jiménez E., Abderrafi K., Abargues R., Valdés J.L., Martínez -Pastor J.P. *Langmuir*, **26**, 7458 (2010).
14. Simakin A.V., Voronov V.V., Shafeev G.A. *Trudy IOFAN*, **60**, 83 (2004).
15. DongShi Zhang, Jun Liu, ChangHao Liang. *Sci. China-Phys. Mech. Astron.*, **60**, 074201 (2017). DOI: 10.1007/s11433-017-9035-8.
16. Yang G.W. *Prog. Mater. Sci.*, **52** (4), 648 (2007).
17. Karpukhin V.T., Kazaryan M.A., Protasov M.V., Malikov M.M., Borodina T.I., Valyano G.E., Gololobova O.A. *Kratk. Soobshch. Fiz. FIAN*, **44** (6), 168 (2017). DOI: 10.3103/S1068335617060045.
18. Karpukhin V.T., Malikov M.M., Valyano G.E., Borodina T.I., Kazaryan M.A. *Al'tern. Energ. Ekol.*, 13–15, 141 (2018). DOI: 10.15518/isjaee.2018.13-15.141–148.
19. Borodina T.I., Valyano G.E., Karpukhin V.T., Malikov M.M., Kazaryan M.A. *Kratk. Soobshch. Fiz. FIAN*, **47** (7), 3 (2020). DOI: 10.3103/S1068335620070039.